Chalcogenide Letters Vol. 20, No. 12, December 2023, p. 891 - 901

Synthesis and mechanism of MoS_2 and graphene oxide insertion in porous multi metal ion modified MnO_2 nanorods for dye degradation

R. Jothiramalingam*, H. Al-Lohedan, D. M. Al-Dhayan, A. Karami
Chemistry Department, College of Science, King Saud University, P.O. Box2455, Riyadh 11451, Kingdom of Saudi Arabia

Layered structure transition metal chalcogenide compound's such as Molybdenum sulfide (MoS_2) deposition in micro/meso porous architecture of MnO_2 could provide hybrid interesting features. Multivalent MnO_2 is an attractive low cost and toxic free catalytic material for oxidation reaction and electrochemical applications. Non-ionic surfactant implication in mesoporous metal ion modified MnO_2 by deposition of metal chalcogenide is an effective composite for dye degradation applications. The low-cost pre-cursor makes it attractive for large-scale production at industrial scale. Hence, in the present study deals with exploit the mechanism of metal chalcogenide and graphene oxide insertion in porous manganese oxide matrix. The as prepared l surface properties of the Nickel and cobalt doped manganese oxide/MoS_2 composite catalyst have shown effective congo red dye degradation activity. The complete color disappearance appeared after interaction with the composite catalyst.

(Received August 31, 2023; Accepted December 14, 2023)

Keywords: Metal oxide composites, MoS_2, Dye degradation, Catalysis, Nanoparticles

1. Introduction

The development and potential applications of a hybrid nanocomposite structure consisting of layered transition metal chalcogenide compounds like Molybdenum sulfide (MoS_2) deposited into a mesoporous-MnO_2-graphene matrix [1-3]. This composite structure has various potential applications, especially in catalysis and environmental remediation. Hybrid Nanocomposite Structure Involving the deposition of MoS_2 into a mesoporous-MnO_2-graphene matrix [4-8]. This combination could provide unique properties and applications due to the synergistic effects of these materials. MnO_2 as a Catalytic Material can Emphasizing the attractiveness of multivalent MnO_2 as a catalytic material, primarily due to its low-cost precursor material. Incorporating various metal ions into the mesoporous matrix enhances its catalytic potential. Metal ion-doped MnO_2 matrices have been utilized for the degradation of volatile organic compounds and the removal of persistent organic pollutants in water [9-12]. The mentioned composite shows promise for sorption of large dye molecules. Surfactant-Assisted Method for Composite Formation is fascinating route adopted in the present study. A non-ionic surfactant-assisted method has been recently developed to form mesoporous metal ion-modified MnO_2. This method enhances catalytic sorption potential and allows for low-cost production at scale. Low-cost sorbents like the discussed composite structure are appealing for complete dye degradation under sono-photocatalytic processes and for removing heavy metals from industrial wastewater. The deposition of MoS_2 into the mesoporous-MnO_2-graphene matrix was carried out using ultrasonication. X-ray diffraction patterns confirm the formation of the desired MnO2 phase with tunnel structure formation due to nickel and cobalt insertion.

Detailed studies on the thermal stability and structural-property relationships of the prepared catalysts were conducted using various physico-chemical methods. Highlighting the importance of incorporating suitable metal ions into mesoporous metal oxide matrices to act as potential catalysts for degrading large dye molecules [13-16].

* Corresponding author: jrajabathar@ksu.edu.sa
https://doi.org/10.15251/CL.2023.2012.891

Overall, this research showcases the potential of these composite structures in catalysis, environmental remediation, and the treatment of industrial wastewater, particularly in the degradation of dyes and the removal of heavy metals. The combination of transition metal chalcogenides, MnO_2, and graphene in a mesoporous matrix offers a promising avenue for advanced material applications.

In the present study, congo red dye is tested as model compound for catalytic degradation reaction. The Congo red compound has been considered an organic azo dye that causes carcinogenicity and other related detrimental severe effects toward human and aquatic life [9,10]. Hence, the objective of the present study is to develop new additive (MoS_2) deposition on Ni-Co MnO_2 is for dye degradation by sono-catalytic method. In addition to the application study, the detailed textural and morphological characterization of newly developed MoS_2 modified Ni-Co- modified MnO_2 composites have also been demonstrated.

2. Materials and methods

In-Situ Doping of Ni ion and Co ions on MnO_2 Framework carried out as follows: The doping of foreign metal ions on the MnO_2 structure is conducted during the precipitation stage. This involves mixing manganese sulfate with appropriate amounts of nickel and cobalt salt solutions, followed by the dropwise addition of non-ionic polymer surfactant (Triton-100) [17-20]. This process ensures the incorporation of these metal ions into the MnO_2 structure. Fabrication of Ni-Co-MnO2 Powder: After the in-situ doping process, the resulting Ni-Co-MnO2 powder is dried at 110°C and subsequently subjected to ultrasonication for 15 minutes at 20% amplitude power under ultrasonic irradiation. Deposition of MoS_2 onto Ni-Co-MnO2: Following the preparation of the Ni-Co-MnO2 composite, MoS2 is deposited onto it. This involves mixing 5 to 15 wt% of MoS2 with the prepared suspension of Ni-Co-MnO2 in an ethanol medium. The sonocatalytic degradation of Congo Red, chosen as a model toxic pollutant, is the focus of the study. Prior to the sonocatalysis treatment, different composite catalysts are mixed with a dye solution for 10 minutes. The mixed solution is then immediately subjected to ultrasonication for 20 minutes at an ultrasonic amplitude power of 20%.The progress of dye degradation is observed by monitoring the UV-Vis absorbance peak between 400 and 700 nm. Complete decomposition of the dye is observed within15-20 minutes of the reaction time. This methodology demonstrates a comprehensive approach involving the preparation of composite materials (Ni-Co-MnO_2 and MoS_2-deposited Ni-Co-MnO_2), followed by the application of sonocatalysis for the degradation of Congo Red as a model pollutant.

3. Results and discussion

The crystalline phase of prepared material is supported by the d-space values of the Ni-Co-MnO_2 nanocomposite matching those of mesoporous Mn_2O_3 (ICSD-44-0141 and JCPDS-24-0508), as well as the indexing of the hkl plane values [11,12]. Additionally, Figure 1a visually confirms that the in-situ doping of nickel and cobalt ions has altered the crystalline structure of pristine porous MnO_2. In Fig. 1(a) more diffraction peaks are obtained compared to Ni-Co-doped MnO_2. After doping of Nickel and cobalt in octahedral matrix of manganese oxide results in superimpose the pristine crystalline phase. The broad- ending in diffraction peaks of Ni-Co-doped MnO_2 are due to reduced nano particle size. This structural modification could potentially lead to enhanced properties or functionalities for the nanocomposite material. The SEM images of NiCo-MnO_2 show that it forms tiny fibrous nanodisks with a flower-like morphology. The SEM images of MoS_2 nanoparticles show that they are needle-like and are inserted in the nanosheets of MnO2 with a tubular morphology. (Fig. 2)[19–24]. Molybdenum sulfide nanoparticle is more flexibly inserted into the flaky nanosheets.

The process involves the dispersion or aggregation of square and rectangle particles of Ni-Co-MnO_2, likely due to ultrasonication and subsequent thermal treatment. The study focuses on the sonocatalytic degradation of Congo Red, serving as a model toxic pollutant. Here are the steps outlined: Preparation of Composite Catalysts and Sonocatalysis is as follows, different types of

composite catalysts are mixed with a dye solution for 10 minutes before subjecting them to sonocatalysis. The mixture is then directly subjected to ultrasonication for 20 minutes at an ultrasonic amplitude power of 20%.

Complete degradation of the dye is observed within this 20-minute reaction time, monitored by the changes in the UV-Vis absorbance peak within the range of 300-600 nm. After the sonocatalysis process, the recycling activity of the prepared materials is assessed. This involves washing the materials and subsequently drying them at a temperature range of 90-100°C for 24 hours.

This likely involves measuring the amount of dye removed and adsorbed onto the composite catalysts at various time intervals to model the kinetics of the adsorption process. This research involve a comprehensive evaluation of the synthesized materials' effectiveness in degrading Congo Red through sonocatalysis, as well as their recycling capability and adsorption kinetics for the removal of the dye from solutions. This approach aims to assess the practical applications and sustainability of these composite catalysts for environmental remediation processes.

Fig. 1 shows the pattern of Sonocatalytic dye degradation in present various Ni-Co-MnO_2 composite catalyst. Fig. 2 shows the SEM images of prepared composite and forms the beautiful flower like morphology with nanodisk shape due to metal ion insertion into the matrix of porous manganese oxide.

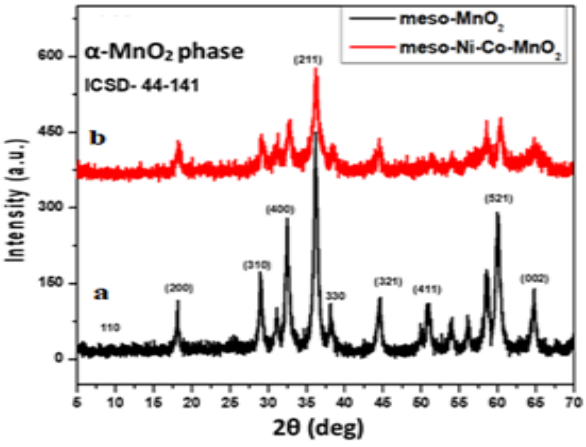

(a)

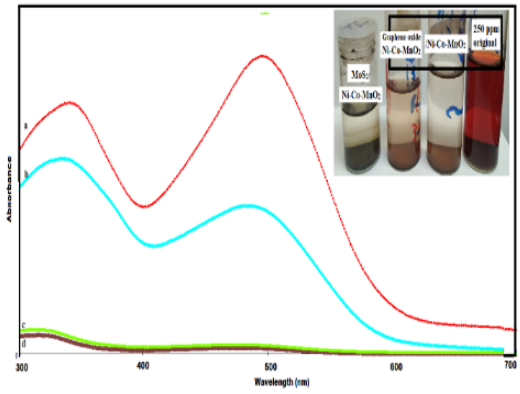

(b)

Fig. 1. XRD diffraction and Congo red dye degradation UV-Visible pattern in the presence of pristine and Ni-Co-MnO_2 composite at different concentration of dye

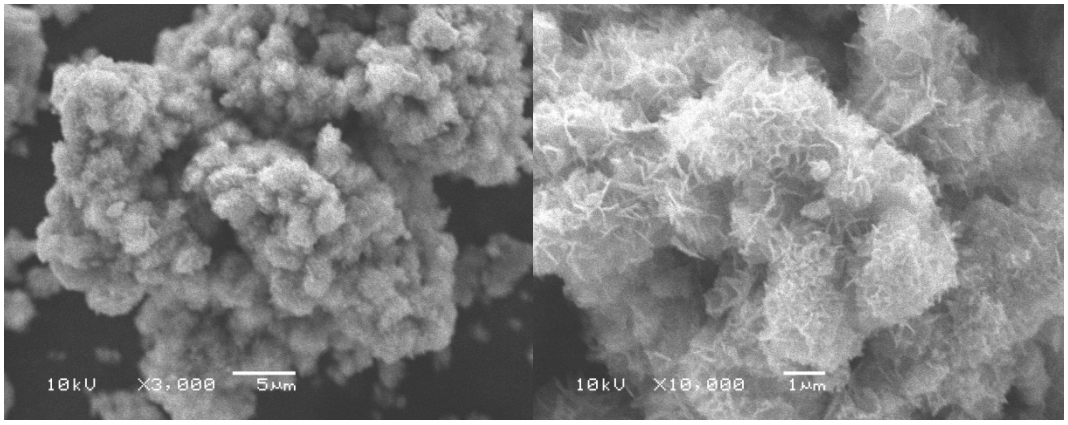

Fig. 2. SEM images of Ni-Co-MnO_2 composite.

This work's main objective is to make additives dispersed Nickel and cobalt doped MnO_2 for effective catalytic applications. The ultrasonic treatment useful for strong dispersion and layer exfoliation process.

In the conducted study, both the addition of additives and the catalytic degradation of the azo dye Congo Red were performed using the ultrasonication method. The process involves heterogeneous solid-liquid interactions in the presence of ultrasonic waves, which can enhance reaction rates. Ultrasonic waves induce various effects that contribute to this enhancement : Increased Reaction Rate via Ultrasonic Waves: Ultrasonic waves promote heterogeneous solid-liquid interactions, potentially leading to increased reaction rates due to the physical modifications induced by the waves. Temperature Increase and Chemical Effects: Ultrasonic waves generate high temperatures upon colliding with the outer surfaces of bubbles in the solution (solution-phase chemistry) and at the liquid-solid interface. This increase in temperature can trigger chemical reactions and accelerate the degradation process. Cavitation Phenomenon and Its Effects: The primary mechanism behind the effects of ultrasound is cavitation. Cavitation refers to the formation, growth, and implosive collapse of microbubbles in the liquid medium due to the pressure fluctuations induced by ultrasound. Production of Free Radicals: During the implosive collapse of microbubbles, significant mechanical forces are generated. These forces can lead to the formation of free radicals due to the extreme conditions during collapse. These free radicals are highly reactive species and play a crucial role in initiating and accelerating degradation reactions. The chemical effects of ultrasound, particularly the production of free radicals through cavitation-induced microbubble collapse, are key contributors to the observed catalytic degradation of the azo dye Congo Red. The combination of physical modifications, increased temperature, and the generation of reactive species contributes to the enhanced degradation efficiency observed in the study.

The free radical/ionic intermediates generated via sono-catalysis could cause a faster rate of reaction. The as-prepared Ni-Co- MnO_2 is first treated with commercially graphene oxide solution in the presence of ultrasonication for 15-20 minutes of reactions. The temperature of the reaction medium was kept between 35 to 40 ^oC. Upon ultrasonication process, the sheet structure of graphene oxide disintegrates as an individual spherical shape with glassy morphology, which is clearly observed HRTEM, Fig. (3 a-b).

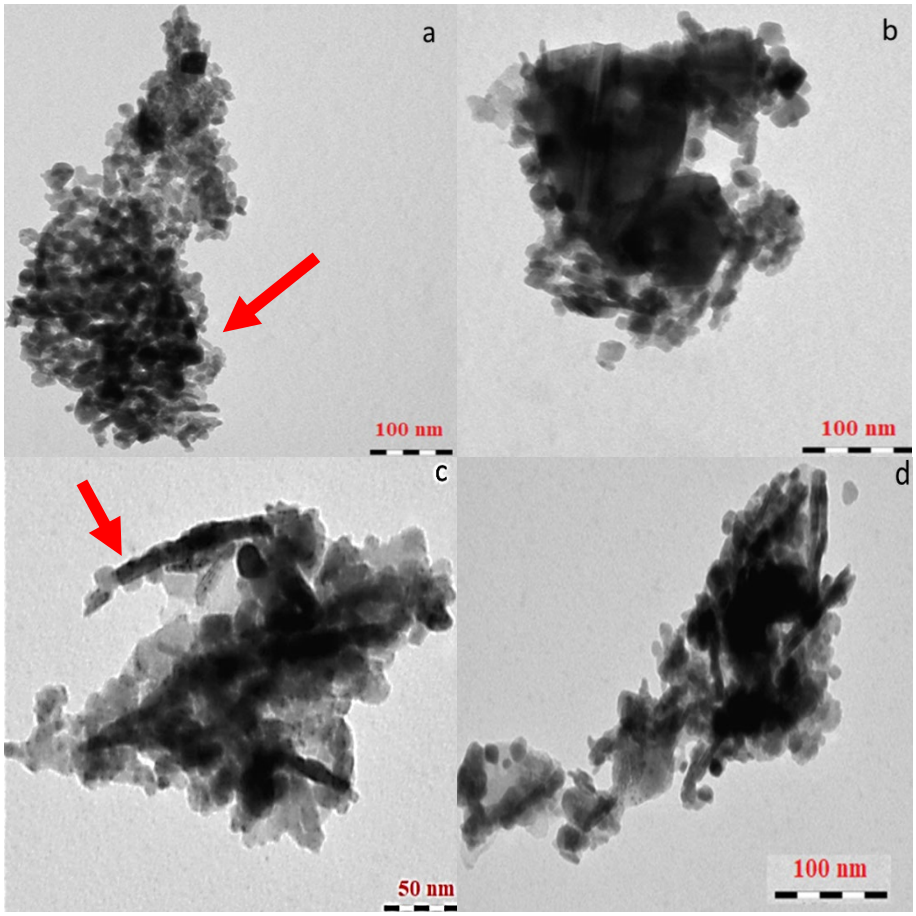

Fig. 3 HR-TEM images of (a-b) Reduced graphene oxide incorporation in Ni-Co-MnOx followed by (c-d) MoS_2 nanofibers dispersion.

Fig. 3b shows Ni-Co-MnO_2 morphology exists in nanorods formation with aggregated spherical shape particles on reduced graphene oxides. Scanning electron micrographs confirms the Before ultrasonication treatment on Ni-Co-MnO_2 forms the pastry nanodisk morphology. The ultrasonication process transforms the pastry morphology into manganese oxide nanorods formation in the presence of graphene oxide exfoliation and reduction process in the presence of sonication causing high heat energy to transform the morphology of the pristine Ni-Co-doped manganese oxide. After the addition of r-graphene oxide into Ni-Co-MnO_2 was further treated with molybdenum sulphide dispersion in the presence of ultrasonication for 10-15 minutes of reaction time. Simple mixing of metal salt addition or metal oxide addition only causes the outer surface dispersion on catalyst support materials. In our present work, additive addition is dispersed on the surface catalyst support. It transforms the morphology. The additive itself transforms its morphology into a different shape with respect to ultrasonication treatment conditions. The same thing happened in our synthesized composite materials. The added MoS_2 nanoparticle transforms into nanofibers and it is interconnected with manganese oxide nanorods inserted in the glassy morphology of reduced graphene oxide. Fig. 3c shows the dark nanofibers (red arrow marked) with manganese oxide tiny nanorods forming spherical and rectangle morphology. In the present method, prepared manganese oxide forms square and rectangle manganese oxide particles due to the presence of framework substituted Ni and cobalt ion substitution in negatively charge MnO_6 octahedral structures. Upon high heat formation in ultrasonic medium, some of weekly bound Ni and Cobalt ions transform in the respective Nickel and Cobalt oxide nanoparticles in the surface of manganese oxide tunnel structures. Thus, that is the reason for the formation of spherical, square, and rectangle particles that exist in the HR-TEM images of as-prepared MoS_2-GO/Ni-Co-MnO_2 composites (Fig. 4). Hence, ultrasonication is not simply utilized to the mixing of the as-prepared mateiral

and it was playing an important role in the transformation texture, morphology and causing the chemical property changes like redox property and electron transport rate for the respective chemical transformations. The graphene-modified Ni-Co-MnO_2 is not shown effective dye absorption due to exfoliation of graphene layer and its depletion nature on the surface of catalyst.

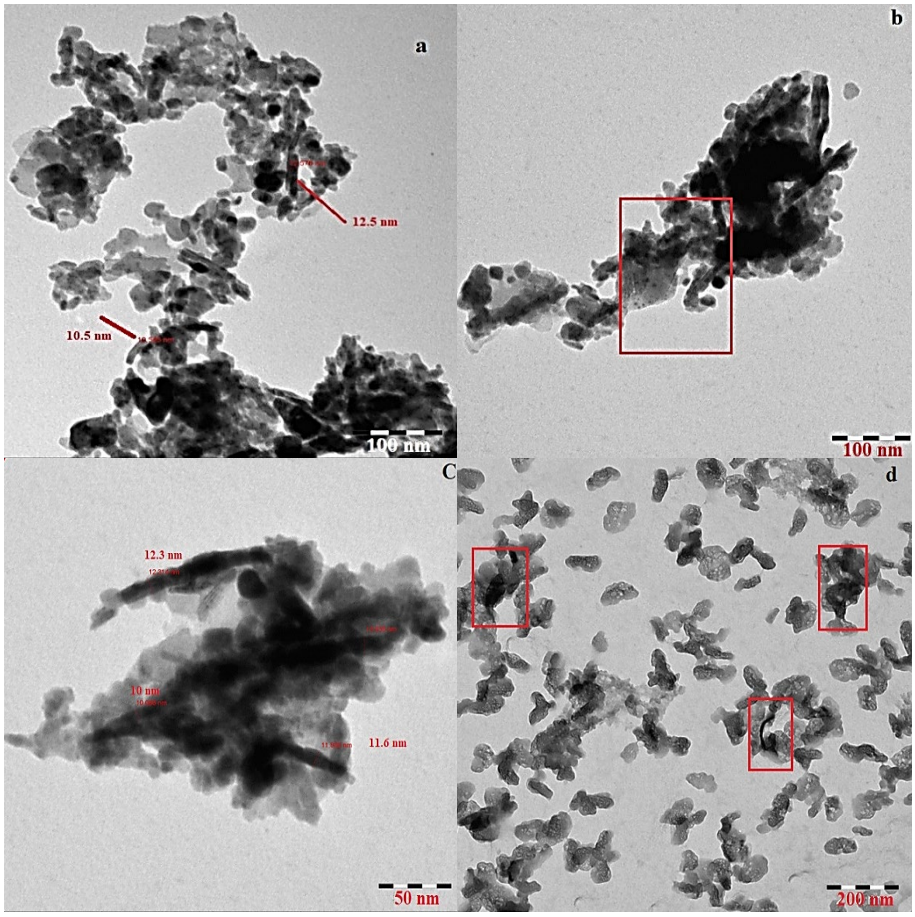

Fig. 4. TEM image of (a-d) 10% MoS_2/Graphene oxide on meso- Ni-Co-MnO_2.

3.1. Textural and morphology characterization of additive modified Ni-Co-MnO_2 composite

The surface area values, and pore size distribution, and pore volume, are given in Table 1. The Type H3 hysteresis is obtained for all additive modified MnO_2 [25]. Type IV isotherm accounts for the neosporosis formation owing to the presence of the mesopores in the prepared Ni-Co-meso-MnO_2.

Table 1. Surface area and pore size parameters of additive modified Ni-Co-MnO_2 nanocomposite.

No.	Sample name	Crystallite size (nm)	BET(m^2/g)	Pore volume(cc/g)	Pore size (nm)
1	Bulk MnO_2	17.3	55	3.36 x 10^{-2}	3.1
2	Ni-Co-MesoMnO_2	15.2	105	0.05061	14.1
3	MoS_2//Ni-Co-MesoMnO_2 with RGO	12.6	92	0.04280	12.85

The as-prepared NiCo-MnO_2, shows large surface area values, such as 105 m^2/g, which is much higher than the commercially and other reported surface area values of MnO_2 (normally surface area obtained below 50 m^2/g). Improved surface area is play a vital role in the sorption process of incoming organic pollutants.

Figure 5 shows the Ft-IR spectra of pristine and MoS_2 modified Ni-Co-MnO_2. The Mn-O stretching frequency of MoSGMn-1 is appeard at 573 cm-1 and 744 cm-1. The other samples are also shows in the same region with slight alteration in their frequency values, MoSGMn-2 shows 566 and 741 cm-1 and MoSGMn-3 show 584 and 750 cm-1 and stretching frequency of 574 and 740 cm-1 obtained for MoSGMn-4.

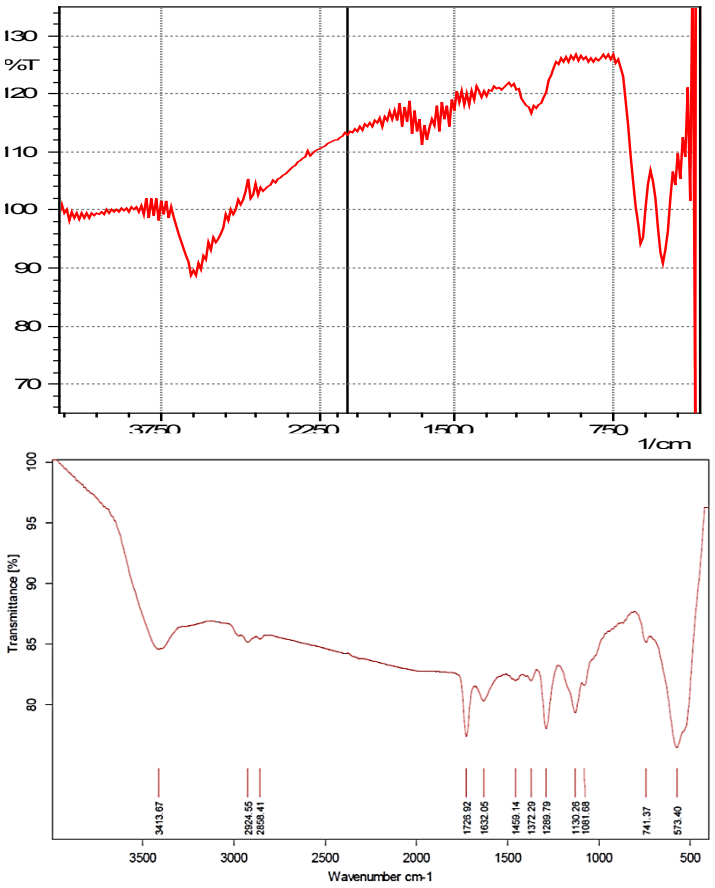

Fig. 5. Ft-Ir spectra of Pristine and MoS_2/graphene oxide coated Ni-Co-MnO_2.

Effect of MoS2 Concentration on Spectral Intensity, Higher amounts of MoS_2 (100 mg and 75 mg) added to r-GO-meso manganese oxide show more intense vibration peaks between 500-700 cm^-1 compared to samples with lower amounts of MoS_2. Samples with lower MoS2 addition exhibit broadened Mn-O stretching peaks (MoSGMn-3 and 4). Potential Improvement in Ionic Transport via the addition of a higher amount of MoS_2 into the manganese oxide matrix appears to facilitate better penetration of MoS_2 into the oxide matrix. This penetration potentially improves or facilitates the ionic transport process during electrochemical reactions, suggesting enhanced electrochemical performance. Identification of Chemical Elements and Functional Groups: Analysis indicates the presence of various chemical elements and functional groups within the composite.
Mo-S-Mo, C-C, C-O stretching frequencies are observed, indicating the presence of MoS_2, graphene oxide, and other constituents in the composite. The S-Mo-S stretching frequency typically falls within the range of 1600-1700 cm^-1 [31,32], characteristic of MoS_2. A broad peak observed at 3412 cm^-1 corresponds to the presence of hydroxyl groups in the as-prepared nanocomposite. Implications for Composite Structure and Properties: The spectral analysis provides insights into

the distribution and interaction of different components within the nanocomposite. Understanding the interaction between MoS_2, r-GO, and mesoporous manganese oxide is crucial for optimizing composite properties and performance in various applications, particularly in electrochemical processes.In summary, the analysis suggests that adjusting the concentration of MoS2 within the composite affects the spectral features and potentially influences the composite's structure, facilitating improved ionic transport and indicating the presence of essential functional groups for specific applications, such as in electrochemical reactions.

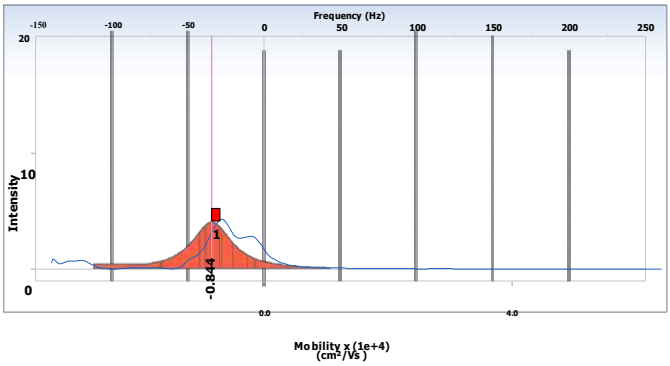

Measurement Results

Zeta Potential	: -63.07	(mV)	Doppler shift	: -34.36	(Hz)
Mobility	: -8.438e-005	(cm²/Vs)	Base Frequency	: 128.8	(Hz)
Conductivity	: 0.0071	(mS/cm)	Conversion Equation	: Huckel	

(a)

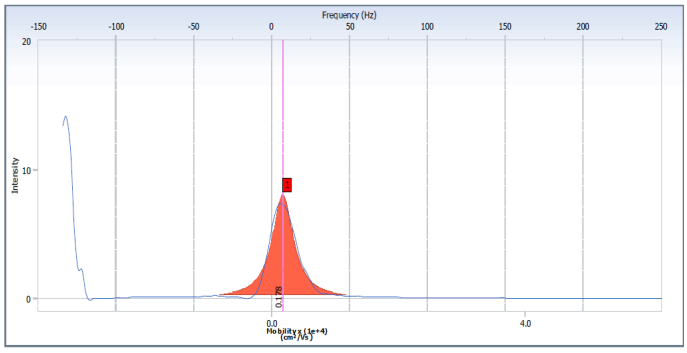

Mesurment Result

Zeta Potential	: 13.33	(mV)	Doppler shift	: 7.27	(Hz)
Mobility	: 1.784e-005	(cm²/Vs)	Base Frequency	: 123.3	(Hz)
Conductivity	: 0.0075	(mS/cm)	Conversion Equation	: Huckel	

(b)

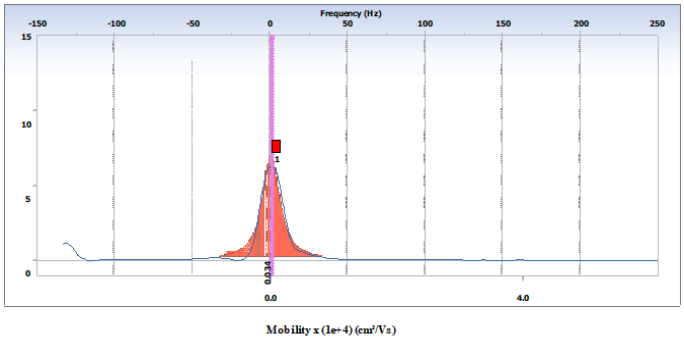

Measurement Results

Zeta Potential	: 2.54	(mV)	Doppler shift	: 1.38	(Hz)
Mobility	: 3.393e-006	(cm²/Vs)	Base Frequency	: 127.4	(Hz)
Conductivity	: 0.0114	(mS/cm)	Conversion Equation	Huckel	

(c)

Fig. 6. Zeta potential measurement of (a) Ni-$CoMnO_2$ (b) Graphene/Ni-$CoMnO_2$ (c) MoS_2-Graphene oxide /Ni-$CoMnO_2$.

The particle size analysis of the prepared composite materials were done by Nano plus analyzer in aqueous medium. The number and volume distribution of particle of as-prepared nanocomposite are 286 (NiCo-mesoMnO_2), and 241 (Go-NiCo-mesoMnO_2) are shown in Fig. 6. Interesting observations are made while measuring zeta potential, and the same is shown in Figure 6 (a-c). The zeta potential values of Ni-CO-meso-MnO2, GO -NiCo-MnO2, and MoS2 modified GO -NiCo-MnO2, highlights that the zeta potential values are negative for Ni-CO-meso-MnO2 and positive for the additive-modified composite samples. Additionally, the incorporation of additives into the MnO2 framework alters the conductivity and electron transport mobility. Specifically, the zeta potential of GO -NiCo-MnO2 is 13.33, while after MoS2 modification, the zeta potential value drops to 2.92.

These observations suggest that the zeta potential values and the incorporation of additives significantly impact the properties of the MnO_2-based materials. The negative zeta potential of Ni-CO-meso-MnO_2 indicates its hydrophilic nature, while the positive zeta potential of the additive-modified composite samples suggests their hydrophobic character. Furthermore, the modification of GO -NiCo-MnO_2 with MoS_2 alters its zeta potential value, potentially influencing its interactions with other materials. The changes in conductivity and electron transport mobility upon additive incorporation can be attributed to alterations in the electronic structure and charge distribution of the MnO_2 framework. These modifications can lead to enhanced or hindered electron transport, depending on the specific additive and its interactions with MnO_2.

SEM images of NiCo-MnO_2 are forms the tiny fibrous nanodisk with flower-like morphology with spherically aggregated particles (Fig. 4).

The catalytic dye degradation run on different cycle have been studied and the same is shown in Figure. 6. The reused catalyst of MoS_2-modifed Ni-Co-MnO2 shown the very effective catalytic activity after various cycle of congo red dye degradation reactions. Hence, as prepared chalcogenide modified porous manganese oxide could be the potential oxidation catalyst for industrial waste water treatment applications.

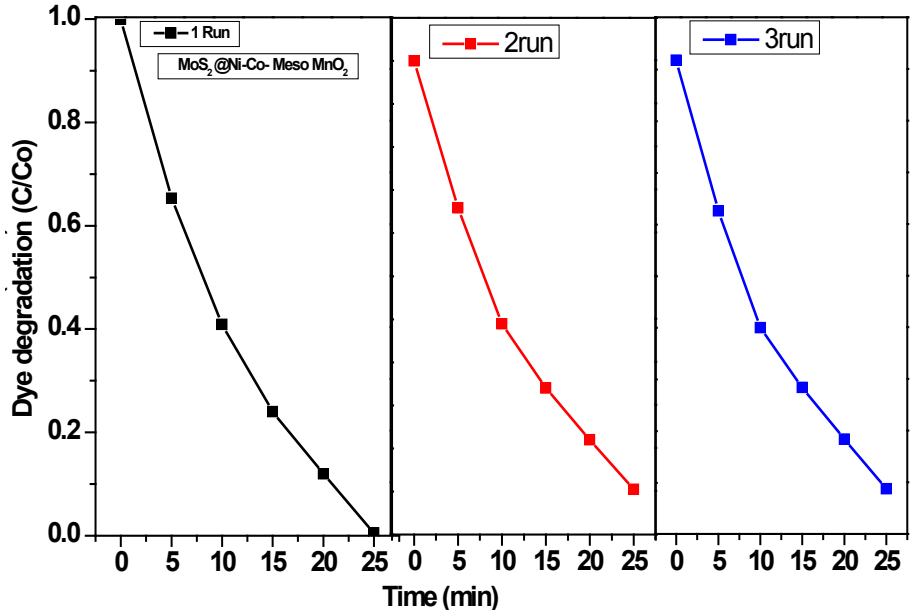

Fig. 7. Effect of MoS_2/Ni-Co-MnO_2 nano composite catalyst test of 5%MoS_2@ Ni-Co-MnO_2 towards complete dye degradation process in the presence of ultraonsic treatment.

4. Conclusions

The complete surface and textural property of as prepared catalysts have been demonstrated. The addition of metal chalcogenides, such as MoS_2, to Ni-Co-MnO_2 nanocomposites can significantly enhance the sonocatalytic activity for dye degradation. This is due to the synergistic effect between the metal oxides and the metal chalcogenides, which leads to the formation of active sites that can generate more reactive oxygen species (ROS) under ultrasound irradiation. The ROS can then attack and degrade the dye molecules.

The study also found that the higher the concentration of MoS_2, the better the sonocatalytic activity. This is because MoS_2 has a high specific surface area and a large number of active sites. Additionally, MoS_2 can act as an electron donor, which can help to promote the formation of ROS. Overall, this study demonstrates that the addition of metal chalcogenides to Ni-Co-MnO2 nanocomposites is a promising strategy for enhancing sonocatalytic dye degradation. This technology could be used to develop more effective wastewater treatment methods for the textile industry. The size and morphology of the nanocomposites can also affect the sonocatalytic activity. For example, smaller nanocomposites with a higher surface area tend to be more active. The sonication parameters, such as the frequency and amplitude of the ultrasound, can also affect the sonocatalytic activity. Hence, the prepared catalyst could act as potential low-cost materials for pollution treatment in dye industrial waste water applications.

Acknowledgements

The authors acknowledge the financial support through Researchers Supporting Project number (RSP2023R354), King Saud University, Riyadh 11451, Saudi Arabia.

References

[1] M. Abecassis-Wolfovich, R. Jothiramalingam, M. V. Landau, M. Herskowitz, B. Viswanathan, T.K. Varadarajan, Appl. Catal. B Environ. 59 (2005) 91-98; https://doi.org/10.1016/j.apcatb.2005.01.001

[2] R. Jothiramalingam, B. Viswanathan, T. K. Varadarajan, Eurasian Chem. J. 6 (2004) 117-122; https://doi.org/10.18321/ectj599

[3] R. Jothiramalingam, B. Viswanathan, T. K. Varadarajan, Catal. Commun. 6 (2005) 41-45; https://doi.org/10.1016/j.catcom.2004.10.008

[4] R. Jothiramalingam, T. M. Tsao, M. K. Wang, Kinet. Catal. 50 (2009) 741-747; https://doi.org/10.1134/S0023158409050164

[5] R. Jothiramalingam, M.K. Wang, J. Hazard. Mater. 147 (2007) 562-569; https://doi.org/10.1016/j.jhazmat.2007.01.069

[6] R. Jothiramalingam, B. Viswanathan, T. K. Varadarajan, J. Mol. Catal. A Chem. 252 (2006) 49-55; https://doi.org/10.1016/j.molcata.2006.01.054

[7] R. J. Ramalingam, N. Konikkara, H. Al-Lohedan, D. M. Al-dhayan, L. J. Kennedy, S. K. K. Basha, S. R. M. Sayed, Int. J. Hydrogen Energy. 43 (2018) 17121-17131; https://doi.org/10.1016/j.ijhydene.2018.07.061

[8] R. Jothi Ramalingam, P. Arunachalam, M. S. Amer, Z. A. AlOthman, A. G. Alanazi, M. M. AL-Anazy, H. A. AL-Lohedan, W. Mohammed Dahan, Intermetallics. 131 (2021) 107101; https://doi.org/10.1016/j.intermet.2021.107101

[9] J. Wang, T. Huang, W. Yin, Energy Technol. 5 (2017) 2055-2064; https://doi.org/10.1002/ente.201700154

[10] X. Shi, Z. Liu, Y. Zheng, G. Zhou, Colloids Surfaces A Physicochem. Eng. Asp. 522 (2017) 525-535; https://doi.org/10.1016/j.colsurfa.2017.03.045

[11] S. Zhu, Q. Shan, F. Dong, Y. Zhang, L. Zhang, Gold Bull. 50 (2017) 61-68;

https://doi.org/10.1007/s13404-017-0196-x
[12] N. Wang, P. Zhao, K. Liang, M. Yao, Y. Yang, W. Hu, Chem. Eng. J. 307 (2017) 105-112; https://doi.org/10.1016/j.cej.2016.08.074
[13] M. S. Kolathodi, M. Palei, T. S. Natarajan, G. Singh, Nanotechnology. 31 (2020); https://doi.org/10.1088/1361-6528/ab5d64
[14] R. M. Obodo, A. C. Nwanya, C. Iroegbu, I. Ahmad, A. B. C. Ekwealor, R. U. Osuji, M. Maaza, F. I. Ezema, Int. J. Energy Res. (2020); https://doi.org/10.1002/er.5416
[15] A.-Y. Lo, L. Saravanan, C.-M. Tseng, F.-K. Wang, J.-T. Huang, ACS Omega. 5 (2020) 578-587; https://doi.org/10.1021/acsomega.9b03163
[16] A. Achour, A. Guerra, F. Moulaï, M. Islam, T. Hadjersi, I. Ahmad, S. Parvez, R. Boukherroub, J.-J. Pireaux, Mater. Chem. Phys. 242 (2020); https://doi.org/10.1016/j.matchemphys.2019.122487
[17] P. Borthakur, M.R. Das, J. Colloid Interface Sci. 516 (2018) 342-354; https://doi.org/10.1016/j.jcis.2018.01.050
[18] J. Z. Zhang, Y. Yan, Chem. Eng. 95 (2019) 405-415; https://doi.org/10.1016/j.jtice.2018.08.006
[19] J. R. Rajabathar, P. Arunachalam, H. A. AL-Lohedan, R. Thankappan, J. N. Appaturi, T. Pulingam, W. Mohammed Dahan, J. Sol-Gel Sci. Technol. 97 (2021) 638-650; https://doi.org/10.1007/s10971-021-05468-3
[20] R. Jothi Ramalingam, P. Arunachalam, J. N. Appaturai, P. Thiruchelvi, Z. A. Al-othman, A. G. Alanazi, H. A. Al-lohedan, J. Alloys Compd. 859 (2021) 158263; https://doi.org/10.1016/j.jallcom.2020.158263
[21] J. R. Rajabathar, P. Arunachalam, Z. A. Issa, T. A. M, Optik (Stuttg). 224 (2020) 165538; https://doi.org/10.1016/j.ijleo.2020.165538
[22] R. J. Ramalingam, H. Al-Lohedan, A. M. Tawfik, G. Periyasamy, M. R. Muthumareeswaran, Chalcogenide Lett. 17 (2020) 423-428; https://doi.org/10.15251/CL.2020.178.423
[23] R. J. Ramalingam, H. A. Lohedan, M. D. Al-Dhayan, S. N. Ibrahim, S. R. M. Syed, J. Ovonic Res. 16 (2020) 1-9; https://doi.org/10.15251/JOR.2020.161.1
[24] R. J. Ramalingam, H. Al-Lohedan, A. M. Tawfik, G. Periyasamy, M. R. Muthumareeswaran, Chalcogenide Lett. 17 (2020) 423-428; https://doi.org/10.15251/CL.2020.178.423
[25] S. J. M. Rosid, S. Toemen, W. A. Wan Abu Bakar, A. H. Zamani, W. N. A. Wan Mokhtar, J. Saudi Chem. Soc. 23 (2019) 284-293; https://doi.org/10.1016/j.jscs.2018.08.002